

Revisiting Beamforming Design for Stable Millimeter-Wave Communications Under Blockages

Kanta Terui, *Graduate Student Member, IEEE*, Kabuto Arai, *Graduate Student Member, IEEE*,
and Koji Ishibashi, *Senior Member, IEEE*

Abstract—This study examines analog beamforming designs utilizing multi-panel arrays for millimeter-wave (mmWave) communication systems under stochastic path blockages where each panel is an integrated circuit that includes power amplifiers, a limited number of antenna elements, and the corresponding phase shifters. In existing commercial mmWave systems, analog beams are typically designed by leveraging all panels cooperatively to align with the line-of-sight (LoS) path, thereby maximizing array gain. Although this beam design is effective in static channels, it is highly susceptible to frequent link disconnections caused by sudden path blockages. To address this challenge, the present study revisits the design of analog beamforming and proposes a multi-beam approach using multi-panel arrays to enhance robustness to path blockages. To evaluate the performance of the multi-beam with multimodal directivity, a theoretical analysis of the outage probability of the spectral efficiency (SE) is conducted. To design the optimal multi-beam based on the derived outage probability, we formulate a panel allocation problem to determine the assignment of panels to specific paths, including both LoS and non-line-of-sight (NLoS) paths. Numerical simulations confirm that the optimal beam, at high target SE, comprises a single sharp beam aligned to the LoS path to maximize array gain, whereas the optimal beam at low target SE is a multi-beam aligned to both the LoS and NLoS paths to acquire spatial diversity. These results demonstrate that the proposed multi-beam design, which utilizes multiple paths, effectively enhances the stability of mmWave communications while ensuring a minimum required performance level.

Index Terms—Millimeter-wave, multi-panel array, beamforming, path blockage, outage minimization.

I. INTRODUCTION

THE demand for wireless communication has seen unprecedented growth with the advent of beyond fifth-generation mobile communications systems (B5G) and sixth-generation mobile communications systems (6G) systems [1]. These systems are envisioned to support a massive increase in data traffic while enabling ubiquitous connectivity among devices and users. For instance, applications such as autonomous vehicle control, remote medical procedures, and industrial internet of things (IIoT) require the stable exchange of large volumes of data, including high-definition video streams [2]–[4]. Achieving stable, high data rate communication under such conditions is critical to fulfilling these demands. Among the various approaches, the use of millimeter-wave (mmWave) frequency bands has garnered significant attention due to

its potential to provide wider bandwidths, thereby enhancing throughput. However, mmWave communications face challenges such as severe path loss caused by water vapor absorption and signal attenuation due to reflection and diffraction, leading to significant degradation in received power [5]. To mitigate these challenges, the inherent short wavelength of mmWave signals enables the deployment of large-scale antenna arrays capable of implementing high-gain beamforming to compensate for path loss [6], [7].

In practical systems, large-scale arrays are often implemented as multi-panel arrays where each panel is an integrated circuit that includes power amplifiers, a limited number of antenna elements, and the corresponding phase shifters [6], [8]–[11]. This approach reduces circuit design costs and minimizes power consumption, allowing for industrial deployment. Furthermore, to address the cost associated with analog-to-digital converter (ADC) design, the antenna array are commonly adopted with a single radio-frequency (RF) chain, requiring analog beamforming techniques.

Current beamforming designs for mmWave systems often rely on codebook-based approaches, where pre-designed codebooks are used to select beams that align with the line-of-sight (LoS) path between a base station (BS) and a user equipment (UE) to acquire high array gain [12]–[14]. While this approach is effective for maximizing received power under static channel conditions, practical mmWave channels are highly susceptible to sudden path blockages caused by obstacles such as pedestrians, vehicles, or falling leaves [15]–[21]. Such dynamic changes due to blockages causes beam misalignment for the selected beam from the codebook, which is aligned to only the LoS path, resulting in an unstable communication system with frequent disconnections. The frequent reconfiguration of beams to reestablish the communication link requires additional overhead, which hinders the overall system performance.

Numerous studies have addressed the issue of mitigating the impact of path blockage in mmWave communications [22]–[32]. The authors in [22]–[25] proposed an optimal beam design to minimize the outage probability of the spectral efficiency (SE), used as a metric for communication stability under path blockage in coordinated multi-point (CoMP) systems. However, directly apply these methods in practical mmWave systems is challenging, because these studies assumed that analog beams can be freely designed with only an equal amplitude constraint, without relying on predefined codebook-based beams commonly used in commercial systems. Moreover, computational complexity poses a significant challenge, because these methods have to solve the optimization problem at every channel coherence time to design beams using

instantaneous channel state information (CSI). Especially, the dominant complexity is in the computation of the outage probability of the SE, which is the objective function in the optimization, because the outage probability is empirically computed via Monte Carlo computations without analytical expressions.

To focus on practical mmWave systems under blockage, the authors in [26]–[28] investigate the effects of path blockage and beam design to address the issue in practical systems. These works claim that leveraging multiple paths, including not only the LoS path but also non-line-of-sight (NLoS) paths, can achieve spatial diversity and enhance communication stability in the presence of path blockage. The works in [27], [28] have proposed multi-beam design where the designed multiple beams are aligned to both the LoS and the NLoS path to achieve spatial diversity. The effectiveness of leveraging multiple paths through the multi-beam design is validated numerically and experimentally, demonstrating the feasibility of achieving stable communication systems. However, the evaluations in these works are limited in simple scenarios with only two paths including a LoS path and a single NLoS path, for the sake of simplifying the performance evaluation and multi-beam design.

To further extend multi-beam design in more practical scenarios, the authors in [29] proposed a multi-beam design with multi panel arrays relying on codebook-based beams. By independently controlling each panel in a multi-panel array, multiple beams aligned to both the LoS path and multiple NLoS paths can be designed, reducing the outage probability and leading to stable communication. However, this method uses a naive multi-beam design with equal panel allocation for each path, without considering outage probability optimization, and lacks theoretical analysis for the multi-beam design.

Considering the aforementioned challenges, we propose analog beamforming designs with multi panel arrays under blockages for stable mmWave communications. The main contributions of the article are summarized as follows:

- **Theoretical analysis of the SE:** The CDF and outage probability of the SE, when using the multi-beam design with the multi-panel array, is derived in closed form. Based on an approximation of array responses [33], the equivalent channel, including analog beams and blockage effects, can be simplified for analytical tractability. Owing to the approximation, the distribution of the equivalent channel can be represented as a Bernoulli-Gaussian mixture distribution, which is composed of the weighted summation of a delta function and multiple Gaussian distributions, where the variance of each distribution depends on the beamforming and blockage effects. Using this distribution, the outage probability of the SE and received signal-to-noise ratio (RSNR) can be derived in closed form.
- **Optimization for panel allocation:** Based on the derived outage probability, we propose two analog beamforming designs: one that considers only the minimization of the outage probability and another that considers both the outage probability and the average SE. To design the optimal multi-beam, we formulate a panel allocation

problem to determine the allocation of panels to specific paths, including both LoS and NLoS paths. Although the panel allocation problem is formulated as a combinatorial optimization, it is feasible to solve the problem with reasonable complexity even when using brute force search, which can obtain global optima. This is because the parameters affecting the complexity such as the number of panels and the number of paths are relatively small values in practical mmWave systems. Unlike the conventional approaches [22]–[25], we can derive the outage probability in closed form without Monte Carlo computation, which reduces the computational complexity for analog beam design. Moreover, the proposed panel allocation algorithm requires only long-term statistics, such as the number of paths and the Rician K -factor, without the need for instantaneous CSI. Thus, the optimization problem does not need to be solved at every channel coherence time, which significantly simplifies the implementation.

Through computational simulations, we evaluate the effectiveness of the theoretical analysis and the proposed optimal beam design with realistic millimeter-wave parameters. The simulation results reveal that the conventional LoS concentrated beam design, while optimal for maximizing the average SE, frequently causes outages of the the target SE, leading to unstable communications. In contrast, the proposed multi-beam design, which utilizes both LoS and NLoS paths, can suppress the outage probability compared to the conventional method.

The structure of this paper is outlined as follows. Section II describes the system model, including the transmission frame, channel model and path blockage model, and the received signal, and Section III describes an overview of the analog beamforming design with multi-panel arrays. In Section IV, the cumulative distribution function (CDF) of the SE is analytically derived for data transmission using a multi-panel array. The proposed beam design considering the outage probability and the average SE is detailed in Section V. In Section VI, the validity of the theoretical analysis is demonstrated, followed by clarifying that the proposed beam design leads to stable communication through computer simulations. Finally, the conclusions of this study are presented in Section VII.

Notation: The following notations are used in this paper. Bold uppercase \mathbf{X} , bold lowercase \mathbf{x} , and non-bold lowercase x are used to denote a matrix, a column vector, and a scalar value, respectively. The imaginary unit is defined as $j = \sqrt{-1}$. $(\cdot)^T$, $(\cdot)^H$, $(\cdot)^*$, $|\cdot|$ and $\|\cdot\|_0$ denote the transpose, conjugate transpose, conjugate, absolute value, and ℓ_0 norm respectively. $\mathbb{E}[\cdot]$ and \otimes are operators of expectation and convolution. $\mathbf{a} \circ \mathbf{b}$ denotes the Hadamard product between \mathbf{a} and \mathbf{b} . $f_X(x)$, $F_X(x)$ denote the probability density function (PDF) and CDF for the random variable x . Especially, $\mathcal{CN}(x; \mu, v)$, $\mathcal{B}(x; p)$, and $\mathcal{U}(x; a, b)$ denote the circularly symmetric complex Gaussian distribution with mean μ and variance v , the Bernoulli distribution with probability p , and the uniform distribution between a and b , respectively. Moreover, $\mathcal{CN}(\mu, v)$, $\mathcal{B}(p)$ and $\mathcal{U}(a, b)$ represent random variables following the circularly symmetric complex Gaussian distribution with mean μ and

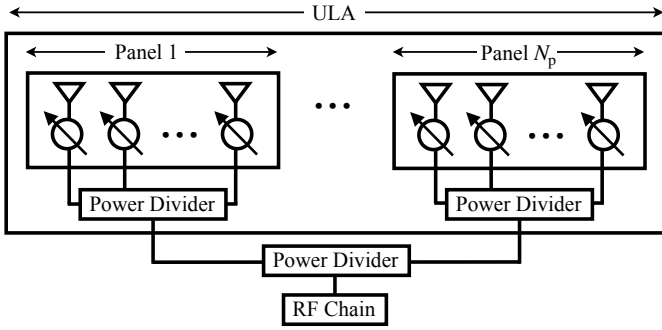


Fig. 1: The BS structure with multi-panel array. Each panel, consisting of a ULA, is connected to a single RF chain through power dividers.

variance v , the Bernoulli distribution with probability p , and the uniform distribution between a and b .

II. SYSTEM MODEL

Consider a point-to-point between a single antenna UE and a BS. The BS is configured as a multi-panel array composed of N_p panels. Each panel is consisted of a uniform linear array (ULA) with N_a antenna elements and all panels are connected to a single RF chain through power dividers. As a result, the entire set of panels constitutes the ULA with a total of $N_t = N_a N_p$ elements. The inter-panel and inter-element spacing is assumed to be set to half a wavelength, and phase calibration is assumed to be perfect, based on the prior works [34]–[37]. Under these conditions, the BS can independently generate multiple beams with each panel. Moreover, as described above, assuming ideal phase calibration, the panels can be coordinated to align their directions to design a single sharp beam with one main lobe, or their directions can be independently controlled to design a multi-wide beam with multiple main lobes.

This paper assumes a transmission frame consisting of two phases: the training phase and the transmission phase. In the training phase, beam sweeping is performed using pre-designed candidate beams in a codebook to estimate the mmWave channel. Based on the estimated CSI, the analog beam is designed for the subsequent transmission phase. To consider training overhead in the beam sweep, the analog beam remains fixed during the transmission phase without updates. It is noted that the equivalent channel response observed in the digital domain can be continuously tracked by baseband signal processing using pilot signals inserted in the transmission phase. Thus, in the transmission phase, a beam misalignment between the designed beam and the actual channel occurs due to the path blockages caused by the movement of obstacles such as pedestrians, vehicles, or falling leaves. In the following subsections, we describe the mmWave channel model in the training and transmission phases, and the received signal model in the transmission phase.

A. Wireless Channel Modeling

1) *Channel Model at the Training Phase:* MmWave channel at the training phase can be model as [38]

$$\hat{\mathbf{h}} = \sum_{l \in \mathcal{L}} g_l \mathbf{a}(N_t, \theta_l) = \mathbf{A}(\boldsymbol{\theta}) \mathbf{g} \in \mathbb{C}^{N_t}, \quad (1)$$

where $L, l \in \mathcal{L} \triangleq \{1, 2, \dots, L\}$ and $\theta_l \in [0, \pi)$ represent the number of paths, a path index and angle of departure (AoD) at the l -th path. In the subsequent discussion, $l = 1$ and $l \geq 2$ are LoS and NLoS path index, respectively. $\mathbf{a}(N, \theta) \triangleq [1, e^{j\pi \cos \theta}, \dots, e^{j\pi(N-1) \cos \theta}]^T \in \mathbb{C}^N$ and $\mathbf{A}(\boldsymbol{\theta}) \triangleq [\mathbf{a}(N_t, \theta_1), \mathbf{a}(N_t, \theta_2), \dots, \mathbf{a}(N_t, \theta_L)] \in \mathbb{C}^{N_t \times L}$ represent array response vector and matrix, where $\boldsymbol{\theta} = [\theta_1, \theta_2, \dots, \theta_L]^T \in \mathbb{R}^L$ is an AoD vector for all paths. Here, g_l denotes the path gain at the l -th path and it is modeled as Nakagami–Rice fading, treated as $g_l \sim \mathcal{CN}(0, \sigma_l^2)$, where σ_l^2 is a variance of the path gain for each path with Rician K -factor κ . The variance σ_l^2 can be defined as

$$\sigma_l^2 \triangleq \begin{cases} \frac{\kappa}{\kappa + 1}, & l = 1 \text{ (LoS)} \\ \frac{1}{\kappa + 1} \frac{1}{L - 1}, & l > 1 \text{ (NLoS)} \end{cases}. \quad (2)$$

Here, the path gain vector is defined as $\mathbf{g} \triangleq [g_1, g_2, \dots, g_L] \in \mathbb{C}^L$. The channel response vector in (1) can be estimated by the training pilots in the beam sweeping precess, based on compressed sensing methods [6], [39], [40]. To focus on the effect of channel fluctuations, this paper assumes that channel estimation in the training phase is ideal without estimation errors. Accordingly, the analog beamforming is determined based on the perfect CSI including AoD vector $\boldsymbol{\theta}$ and the path gain vector \mathbf{g} .

2) *Channel Model at the Transmission Phase:* In the subsequent transmission phase, obstructions may block the paths abruptly [15]–[17]. Channel response vector with stochastic path blockage can be modeled as

$$\mathbf{h} = \sum_{l \in \mathcal{L}} \omega_l g_l \mathbf{a}(N_t, \theta_l) = \mathbf{A}(\boldsymbol{\theta})(\boldsymbol{\omega} \circ \mathbf{g}) \in \mathbb{C}^{N_t}, \quad (3)$$

where $\omega_l \in \{0, 1\}$ is a stochastic binary blockage parameter for the l -th path, and $\boldsymbol{\omega} \triangleq [\omega_1, \omega_2, \dots, \omega_L]^T \in \{0, 1\}^L$ denotes the vector of the blockage parameter. Note that the blockage parameter ω_l is not binary and should be affected by the beam width in practice [19], [20]. The effect of this simplification will be evaluated quantitatively in Section VI.

Path blockages arise stochastically as a result of temporal fluctuation in the communication environment around the BS and UE. According to the literature [22]–[25], blockage parameter ω_l is a Bernoulli random variable with path blockage probability \hat{p} . The probability mass function (PMF) of the \hat{p} is written as $f_{\hat{p}}(\hat{p}) = \mathcal{U}(\hat{p}; p_{\min}, p_{\max})$, where p_{\min} and p_{\max} are minimum and maximum blockage probability, respectively. The PMFs of ω_l and $\boldsymbol{\omega}$, given the blockage probability \hat{p} , are expressed as

$$f_{\Omega_l}(\omega_l | \hat{p}) = \hat{p}^{(1-\omega_l)} (1 - \hat{p})^{\omega_l}, \omega_l \in \{0, 1\}, \forall l, \quad (4a)$$

$$f_{\Omega}(\boldsymbol{\omega} | \hat{p}) = \prod_{l=1}^L f_{\Omega_l}(\omega_l | \hat{p}), \quad (4b)$$

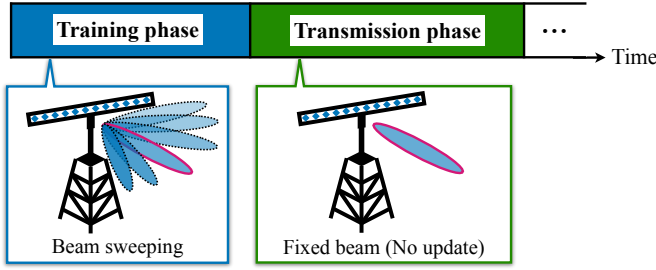


Fig. 2: Illustration of the transmit frame structure and beam design.

By marginalizing (4) over the blockage probability \hat{p} , the PMFs of the blockage parameters can be reformulated as

$$f_{\Omega_l}(\omega_l) = \int f_{\Omega_l}(\omega_l|\hat{p})f_{\hat{p}}(\hat{p})d\hat{p},$$

$$= p_{\text{blk}}^{(1-\omega_l)}(1-p_{\text{blk}})^{\omega_l} = \mathcal{B}(\omega_l; p_{\text{blk}}), \quad (5a)$$

$$f_{\Omega}(\boldsymbol{\omega}) = \prod_{l=1}^L f_{\Omega_l}(\omega_l), \quad (5b)$$

where p_{blk} is an average path blockage probability and defined as $p_{\text{blk}} = (p_{\text{min}} + p_{\text{max}})/2$.

B. Received Signal During the Transmission Phase

In the transmission phase, the received signal y is given as

$$y = \mathbf{h}^H \mathbf{f} s + z = h_{\text{eq}} s + z \in \mathbb{C}, \quad (6)$$

where $\mathbf{f} \in \mathbb{C}^{N_t}$ is an analog beamforming vector designed by estimated CSI, $s \in \mathcal{CN}(0, P_{\text{tx}})$ is a transmit signal with average transmit power P_{tx} , and $z \in \mathcal{CN}(0, \sigma_z^2)$ is an additive white Gaussian noise (AWGN) with noise variance σ_z^2 , respectively. $h_{\text{eq}} \in \mathbb{C}$ is an equivalent channel response including the analog beamforming, which can be written as

$$h_{\text{eq}} \triangleq \mathbf{h}^H \mathbf{f} = (\boldsymbol{\omega} \circ \mathbf{g})^H \mathbf{a}_{\text{eq}}, \quad (7)$$

where $\mathbf{a}_{\text{eq}} \triangleq \mathbf{A}^H(\boldsymbol{\theta}) \mathbf{f} \in \mathbb{C}^L$ is an equivalent array response. Signal-to-noise ratio (SNR) is defined as $\gamma_{\text{tx}} \triangleq P_{\text{tx}}/\sigma_z^2$. In the following section, it is assumed that the equivalent channel response h_{eq} can be ideally estimated using baseband signal processing with pilot signals inserted in the transmission phase¹.

III. ANALOG BEAMFORMING DESIGN

In this section, we introduce the analog beamforming design with multi-panel arrays. By leveraging the structure of the multi-panel array, each panel can independently generate the analog beamforming. Using the estimated CSI at the training phase, the analog beamforming vector $\mathbf{f}_m \in \mathbb{C}^{N_a}$ at the m -th panel can be designed as

$$\mathbf{f}_m = \frac{\psi_m}{\sqrt{N_t}} \mathbf{a}(N_a, \phi_m) \in \mathbb{C}^{N_a}, \quad (8)$$

¹Note that the number of pilots required to estimate h_{eq} is significantly smaller than that needed for beam sweeping because the equivalent channel response h_{eq} is a scalar quantity. Thus, the pilot overhead for baseband channel estimation is negligible.

where ψ_m and ϕ_m denote a phase difference and directivity at the m -th panel, respectively. The phase difference at the m -th panel is defined as

$$\psi_m = \exp\{j\pi(m-1)N_a \cos(\phi_m)\}. \quad (9)$$

Furthermore, we assume that the AoD of each path θ_l can be estimated perfectly with high precision beam sweeping in the training phase. Hence, the BS can generate ideal analog beams aligned with the AoD. By combining the beamforming vectors for each panel as described in (8), the analog beamforming vector \mathbf{f} can be represented as

$$\mathbf{f} = [\mathbf{f}_1^T, \dots, \mathbf{f}_{N_p}^T]^T \in \mathbb{C}^{N_t}. \quad (10)$$

Hereafter, the proposed analog beam design is discussed in detail in comparison with conventional methods. Conventional beamforming designs align all panels cooperatively to form a sharp beam that focuses exclusively on the LoS component of the AoD, θ_1 such that $\phi_m = \theta_1, \forall m \in \{1, \dots, N_p\}$ in (8). In contrast, the proposed method leverages the estimated AoDs of all paths, $\boldsymbol{\theta}$, obtained during the training phase, to enable the design of multiple beams that align with multiple AoDs. Fig. 3 illustrates the beam patterns of the conventional analog beam with a single directionality and the proposed analog beam with multiple directionalities enabled by independent panel control. As shown in the figure, the conventional beam focuses only on the LoS direction with high array gain, leading to frequent communication disconnections if the LoS path is blocked by obstacles. In contrast, the proposed method gains spatial diversity owing to multiple beams aligned with multiple paths, enabling stable communication through the remaining paths even if any path is blocked. However, owing to the trade-off between array gain and spatial diversity, determining the number of panels allocated to each path is essential to improving system performance. To represent the number of panels assigned to each path, the panel allocation vector $\mathbf{q} = [q_1, q_2, \dots, q_L]^T \in \mathbb{Z}^L$ is introduced. $q_l \geq 0$ is the number of panels allocated to the l -th path such that $\sum_{l \in \mathcal{L}} q_l = N_p$. For the sake of future convenience, let N_b denote the number of beams aligned with the selected N_b paths, where N_b satisfies $N_b = \|\mathbf{q}\|_0$.

The panel allocation vector \mathbf{q} is not uniquely determined and must be carefully designed to align with the specific objectives of the system. Therefore, we optimize panel allocation to minimize the outage probability of the SE, which is a metric of communication stability. To formulate the objective function for the outage probability, the distribution of SE should be derived in closed form, which is described in detail in Section IV. The optimization method for panel allocation using the derived outage probability is described in Section V.

IV. THEORETICAL ANALYSIS OF SPECTRAL EFFICIENCY

In this section, we derive the CDF of the SE, when using the multi-beam design with multimodal directivity, in the considered mmWave communication system with the multi-panel array.

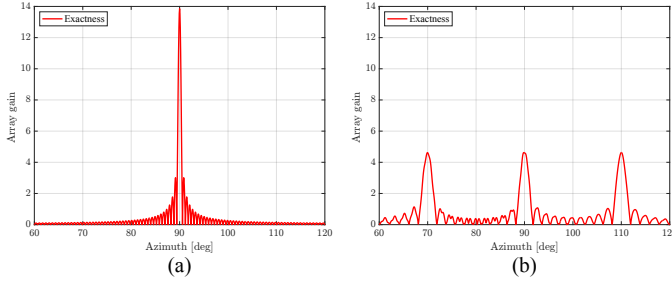


Fig. 3: Comparison of the beam pattern between (a) the conventional single main lobe beamforming with $\mathbf{q} = [N_p, 0, 0]^T$, and (b) the proposed multiple beam with $\mathbf{q} = [2, 2, 2]^T$, where $N_a = 32$, $N_p = 6$.

Based on the received signal model in (6), the SE ξ can be expressed as

$$\xi \triangleq \log_2(1 + \gamma), \quad (11)$$

where γ denotes the RSNR, which can be expressed as

$$\gamma \triangleq \gamma_{\text{tx}} |h_{\text{eq}}|^2 = \gamma_{\text{tx}} |(\boldsymbol{\omega} \circ \mathbf{g})^H \mathbf{a}_{\text{eq}}|^2. \quad (12)$$

To derive the CDF of the SE, the distribution of the equivalent channel h_{eq} must be derived. By applying an approximation [33] for array responses, the distribution of h_{eq} can be approximately derived, as detailed in Section IV-A. From the derived distribution of h_{eq} , the CDF of the SE can be derived, detailed in Section IV-B.

A. Approximation of the Equivalent Array Response

In (12), the equivalent array response $\mathbf{a}_{\text{eq}} = \mathbf{A}^H(\boldsymbol{\theta})\mathbf{f}$ is composed of the inner products between the array responses and the analog beamforming vector, which is also the array response, as shown in (8). To simplify the expression of the inner products for array responses, this paper adopts the following approximation [33], which is valid in large-scale array systems.

$$\mathbf{a}(N_a, \theta)^H \mathbf{a}(N_a, \phi) \approx \begin{cases} N_a, & (\theta = \phi, \text{ main lobe}) \\ 0, & (\theta \neq \phi, \text{ side lobe}) \end{cases}. \quad (13)$$

This approximation implies that the main lobe contains the effective energy, while the remaining parts, including the side lobes, are assumed to be zero as shown in Fig. 4. Using the approximation in (13), the equivalent array response \mathbf{a}_{eq} can be approximated with panel allocation vector \mathbf{q} as

$$\begin{aligned} \mathbf{a}_{\text{eq}} &= [\mathbf{a}(N_t, \theta_1), \dots, \mathbf{a}(N_t, \theta_L)]^H \\ &\quad \cdot \frac{1}{\sqrt{N_t}} [\psi_1 \mathbf{a}(N_a, \phi_1), \dots, \psi_{N_p} \mathbf{a}(N_a, \phi_{N_p})], \\ &\approx \frac{N_a}{\sqrt{N_t}} \mathbf{q}. \end{aligned} \quad (14)$$

As evaluated in the numerical simulation described in Section VI, the effects of the approximation error on the CDF of the SE are negligible.

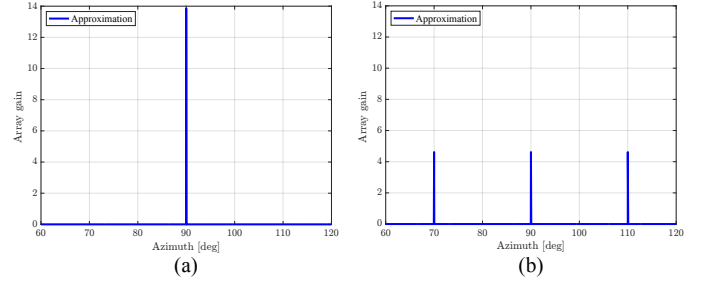


Fig. 4: Comparison of the approximated beam pattern between (a) the conventional beam with $\mathbf{q} = [N_p, 0, 0]^T$, and (b) the proposed multiple beam with $\mathbf{q} = [2, 2, 2]^T$, where $N_a = 32$, $N_p = 6$.

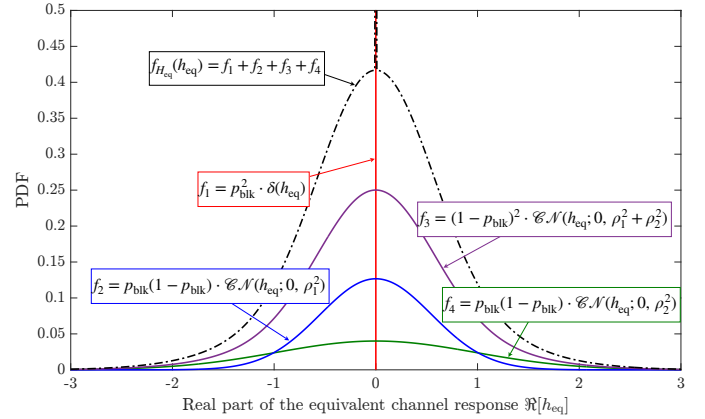


Fig. 5: PDF of the real part of the equivalent channel response $\Re[h_{\text{eq}}]$ with $L = 2$, $N_a = 32$, $N_p = 4$, $p_{\text{blk}} = 0.4$, $\kappa = 10$ [dB], $\mathbf{q} = [2, 2]^T$, $N_b = 2$

B. Derivation of the Equivalent Channel Response and RSNR

Substituting the equivalent array response in (14) into (7), the equivalent channel response h_{eq} can be approximated as

$$h_{\text{eq}} \approx \frac{N_a}{\sqrt{N_t}} \sum_{l \in \mathcal{L}} g_l^* \omega_l q_l = \frac{N_a}{\sqrt{N_t}} \sum_{l \in \mathcal{L}} g_{q_l} \omega_l, \quad (15)$$

where, g_{q_l} is a random variable and can be represented as $g_{q_l} \sim \mathcal{CN}(0, \rho_l^2)$ with variance $\rho_l^2 \triangleq \sigma_l^2 q_l^2$. As shown in equation (15), the random variable of the equivalent channel response h_{eq} is expressed as the sum of the products of the Gaussian random variable g_{q_l} and the Bernoulli random variable ω_l . Therefore, the PDF of h_{eq} becomes the Bernoulli–Gaussian mixture, which is expressed as (16) in the top of next page. The detail of the derivation of (16) is described in Appendix-A. Fig. 5 illustrates the PDF of the equivalent channel response, where the number of path is $L = 2$ with the LoS path and one NLoS path. Because of $L = 2$, there are $2^L = 4$ blockage patterns: 1) both paths are blocked, 2) only the NLoS path is blocked, 3) only the LoS path is blocked, and 4) neither path is blocked. Subsequently, the PDF of the equivalent channel $f_{H_{\text{eq}}}(h_{\text{eq}})$ is expressed as the summation of four distributions f_1, \dots, f_4 corresponding to each blockage pattern, as shown in Fig. 5.

With an approximation of the equivalent channel response h_{eq} in (15), the RSNR γ defined in (12) can also be approxi-

$$f_{H_{\text{eq}}}(h_{\text{eq}}) = p_{\text{blk}}^{N_b} \delta(h_{\text{eq}}) + \sum_{t=1}^{N_b} p_{\text{blk}}^{N_b-t} (1-p_{\text{blk}})^t \left\{ \sum_{1 \leq i_1 < \dots < i_t \leq L} \mathcal{CN} \left(h_{\text{eq}}; 0, \frac{N_a^2}{N_t} \sum_{k=1}^t \rho_{i_k}^2 \right) \right\} \quad (16)$$

$$f_{\Gamma}(\gamma) = p^{N_b} \delta(\gamma) + \sum_{t=1}^{N_b} p^{N_b-t} (1-p)^t \left\{ \sum_{1 \leq i_1 < \dots < i_t \leq L} \frac{1}{\sum_{k=1}^t \rho_{i_k}^2} \exp \left(-\frac{\gamma}{\sum_{k=1}^t \rho_{i_k}^2} \right) \right\} \quad (18)$$

$$F_{\Gamma}(\gamma) \triangleq \int_{-\infty}^{\gamma} f_{\Gamma}(\tilde{\gamma}) d\tilde{\gamma} = p_{\text{blk}}^{N_b} + \sum_{t=1}^{N_b} p_{\text{blk}}^{N_b-t} (1-p_{\text{blk}})^t \left\{ \sum_{1 \leq i_1 < \dots < i_t \leq L} 1 - \exp \left(-\frac{\gamma}{\gamma_{\text{tx}} N_a^2 / N_t \sum_{k=1}^t \rho_{i_k}^2} \right) \right\} \quad (19)$$

mated as

$$\gamma = \gamma_{\text{tx}} |h_{\text{eq}}|^2 \approx \frac{\gamma_{\text{tx}} N_a^2}{N_t} \left| \sum_{l \in \mathcal{L}} g_{q_l} \omega_l \right|^2. \quad (17)$$

As shown in equation (17), the distribution of the RSNR γ can be represented as the squared of random variable of the Bernoulli–Gaussian mixture distribution. The PDF and CDF of the RSNR γ are derived in (18) and (19), respectively. The detailed derivations of (18) and (19) are provided in Appendix-B. Subsequently, by substituting $\gamma = 2^{\xi} - 1$ into (19), the CDF of the SE can be derived in closed form because the logarithm function is a monotonically increasing function.

V. PANEL ALLOCATION METHOD

In this section, we consider three analog beamforming designs using the distributions of the SE derived in Section IV-B. The first method considers only the maximization of the average SE, which is confirmed to be equivalent to the conventional beam design focusing only on the LoS path, as described in Section V-A. The second method considers only the minimization of the outage probability, which is described in Section V-B. The third method considers both the average SE and the outage probability, as described in Section V-C.

A. Average SE Maximization

This subsection formulates the panel allocation problem based on maximizing the average SE. The average SE is defined as $\mathbb{E}[\xi] = \mathbb{E}[\log_2(1 + \gamma)]$. Using the Jensen's inequality [41] because of the strict convexity of the logarithmic function, the average SE is bounded as

$$\mathbb{E}[\xi] = \mathbb{E}[\log_2(1 + \gamma)] \leq \log_2(1 + \mathbb{E}[\gamma]) = \xi_{\text{ave}}, \quad (20)$$

where ξ_{ave} is the upper bound of the average SE corresponding to the SE at the average RSNR $\mathbb{E}[\gamma]$.

For analytical tractability, we maximize the upper bound of the SE ξ_{ave} instead of directly maximizing the average SE $\mathbb{E}[\xi]$. From (20), the maximization of the upper bound ξ_{ave} is equivalent to the maximization of the average RSNR $\mathbb{E}[\gamma]$.

Subsequently, the panel allocation problem to maximize the upper bound is formulated as

$$\underset{\mathbf{q} \in \mathbb{Z}^L}{\text{maximize}} \quad \mathbb{E}[\gamma], \quad (21a)$$

$$\text{subject to} \quad q_l \geq 0, \quad (21b)$$

$$\sum_{l \in \mathcal{L}} q_l = N_p. \quad (21c)$$

From (16), the average RSNR given the random variables ω , denoted as $\mathbb{E}[\gamma|\omega]$, can be expressed as

$$\mathbb{E}[\gamma|\omega] = \gamma_{\text{tx}} \mathbb{E} \left[|h_{\text{eq}}|^2 \mid \omega \right] = \frac{\gamma_{\text{tx}} N_a^2}{N_t} \sum_{l \in \mathcal{L}} \omega_l^2 q_l^2 \sigma_l^2. \quad (22)$$

As each path blockage parameter ω_l is discrete random variable as defined in (4), the average RSNR $\mathbb{E}[\gamma]$ can be calculated by averaging $\mathbb{E}[\gamma|\omega]$ over the random variable ω as (23) in the top of next page, where t denotes the number of non-blocked paths.

From the average RSNR $\mathbb{E}[\gamma]$ in (23), the maximization problem in (21) can be reformulated as

$$\underset{\mathbf{q} \in \mathbb{Z}^L}{\text{maximize}} \quad \kappa(L-1)q_1^2 + q_2^2 + \dots + q_L^2, \quad (24a)$$

$$\text{subject to} \quad q_l \geq 0, \quad (24b)$$

$$\sum_{l \in \mathcal{L}} q_l = N_p. \quad (24c)$$

The objective function of (24) is expressed as a sum of squared allocation variables q_l . As the Rician K -factor κ is typically larger than 1 in practical mmWave communication environments [42], the first term of the objective function in (24a), $\kappa(L-1)q_1^2$ is dominant for the maximization problem. Thus, the optimal solution of the maximization problem (24) can be derived in closed-form as

$$\mathbf{q} = [N_p, 0, \dots, 0]^T. \quad (25)$$

This solution indicates that focusing all panels only on the LoS path can maximize the average RSNR, which corresponds to maximizing the upper bound of the average SE. Therefore, the codebook-based beamforming commonly employed in current mmWave systems is optimal for maximizing the average RSNR.

$$\begin{aligned}
 \mathbb{E}[\gamma] &= \sum_{\boldsymbol{\omega} \in \{0,1\}^{L \times 1}} \mathbb{E}[\gamma|\boldsymbol{\omega}]p(\boldsymbol{\omega}) = p_{\text{blk}}^L + \sum_{t=1}^L p_{\text{blk}}^{L-t}(1-p_{\text{blk}})^t \sum_{1 \leq i_1 < \dots < i_t \leq L} \sum_{k=1}^t q_i^2 \sigma_i^2 \\
 &= \frac{\gamma_{\text{tx}} N_a^2}{N_t(\kappa+1)(L-1)} (1-p_{\text{blk}}) (\kappa(L-1)q_1^2 + q_2^2 + \dots + q_L^2)
 \end{aligned} \tag{23}$$

B. Outage Probability Minimization

To achieve stable communication, it is essential not only to enhance the average value of the SE but also to mitigate the tail of its distribution, corresponding to the occurrence probability of poor SE performance. Therefore, we propose the panel allocation that minimizes the outage probability for a desired target SE. In this paper, the outage probability is defined as

$$p_{\text{out}} \triangleq \Pr\{\log_2(1+\gamma) < \xi_{\text{th}}\}, \tag{26}$$

where ξ_{th} denotes the target SE desired by the UE. Using (26), the panel allocation problem for minimizing the outage probability can be formulated as

$$\underset{q_l, \forall l \in \mathcal{L}}{\text{minimize}} \quad \Pr\{\log_2(1+\gamma) < \xi_{\text{th}}\}, \tag{27a}$$

$$\text{subject to} \quad \sum_{l \in \mathcal{L}} q_l = N_p, \tag{27b}$$

$$q_l \geq 0. \tag{27c}$$

To simplify the analytical tractability, by removing the logarithmic function and focusing on the argument γ , the optimization problem (27) can be reformulated as

$$\underset{q_l, \forall l \in \mathcal{L}}{\text{minimize}} \quad \Pr\{\gamma < \gamma_{\text{th}}\}, \tag{28a}$$

$$\text{subject to} \quad \sum_{l \in \mathcal{L}} q_l = N_p, \tag{28b}$$

$$q_l \geq 0, \tag{28c}$$

where γ_{th} is the target RSNR, defined as $\gamma_{\text{th}} \triangleq 2^{\xi_{\text{th}}} - 1$.

The outage probability in the objective function (28a) is equivalent to the CDF of the RSNR in (19) at $\gamma = \gamma_{\text{th}}$ as

$$\Pr\{\gamma \leq \gamma_{\text{th}}\} = \int_{-\infty}^{\gamma_{\text{th}}} f_{\Gamma}(t) dt = F_{\Gamma}(\gamma_{\text{th}}). \tag{29}$$

By utilizing the CDF of the RSNR derived in (19), the outage probability for any target RSNR can be obtained in closed-form without using the Monte Carlo computation, unlike the conventional approaches [22]–[25]. For the sake of notation convenience, the outage probability in (29) is expressed as a function of the panel allocation vector \mathbf{q} , denoted as

$$f_{\text{out}}(\mathbf{q}) = F_{\Gamma}(\gamma_{\text{th}}|\mathbf{q}). \tag{30}$$

To solve the optimization problem in (28), we propose a panel allocation algorithm based on brute-force search. The pseudocode of the proposed algorithm is provided in Alg. 1.

Algorithm 1 Outage Probability Minimization

Input: $\xi_{\text{th}}, \gamma_{\text{tx}}, N_a, N_t, \kappa, L, p_{\text{blk}}$

Output: $\mathbf{q}^{\text{opt}} \in \mathbb{Z}^L$

- 1: Generate $\tilde{\mathbf{Q}} \in \mathbb{Z}^{L \times C}$ that contains all pattern vectors
 - 2: Calculate \mathbf{q}^{opt} by solving the problem (32)
-

The proposed algorithm in Alg. 1 determines the optimal panel allocation by exhaustively searching all possible combinations of panels and paths. The number of total patterns for panel allocation is given by

$$C = \sum_{q_1=1}^{N_p} \binom{N_p + L - q_1 - 2}{L - 2}. \tag{31}$$

Let us define the panel allocation matrix including all pattern as $\tilde{\mathbf{Q}} = [\tilde{\mathbf{q}}_1, \dots, \tilde{\mathbf{q}}_C] \in \mathbb{C}^{L \times C}$, where $\tilde{\mathbf{q}}_i$ represents the i -th panel allocation candidate among total C patterns. Using the panel allocation matrix $\tilde{\mathbf{Q}}$, the optimal panel allocation vector $\mathbf{q}^{\text{opt}} \in \mathbb{Z}^L$ can be calculated as

$$\mathbf{q}^{\text{opt}} = \underset{\tilde{\mathbf{q}}_i \in \tilde{\mathbf{Q}}}{\text{argmin}} f_{\text{out}}(\tilde{\mathbf{q}}_i). \tag{32}$$

C. Outage Minimization with Reinforcement for Average SE

The proposed algorithm in Alg. 1, described in the previous subsection, considers only minimizing the outage probability. Focusing only on minimizing the outage probability may lead to a significant degradation in the average SE, as will be demonstrated in Section VI. To address this challenge, we enhance the previous algorithm by introducing a modification to mitigate the degradation of the average SE. The pseudocode of this enhanced algorithm is provided in Alg. 2.

Let \tilde{p}_i and p^{min} denote the outage probability corresponding to the i -th panel allocation vector $\tilde{\mathbf{q}}_i$ and the minimum outage probability, which are given by

$$\tilde{p}_i = f_{\text{out}}(\tilde{\mathbf{q}}_i), \quad \forall i \in \{1, 2, \dots, C\}, \tag{33}$$

$$p^{\text{min}} = \min_{i \in \{1, 2, \dots, C\}} \tilde{p}_i. \tag{34}$$

These outage values in (33), (34) can be obtained by Alg. 1. To enhance the average SE performance, the proposed algorithm determines the optimal allocation vector \mathbf{q}^{opt} that maximizes the average RSNR (which corresponds to maximizing the upper bound of the average SE in (20)) from the allocation candidates such that the absolute difference from

Algorithm 2 Outage Probability Minimization with Reinforcement for Average SE

Input: $\xi_{\text{th}}, \gamma_{\text{tx}}, N_a, N_t, \kappa, L, \hat{p}_{\text{blk}}, \varepsilon$
Output: $\mathbf{q}^{\text{opt}} \in \mathbb{Z}^L$

- 1: Generate $\tilde{\mathbf{Q}} \in \mathbb{Z}^{L \times C}$ that contains all pattern vectors
 - 2: Calculate \tilde{p}_i and p^{min} from (33) and (34)
 - 3: Calculate \mathbf{q}^{opt} by solving the problem (35)
-

the minimum outage probability p^{min} is less than or equal to a small value ε . The optimization problem is formulated as

$$\mathbf{q}^{\text{opt}} = \underset{j \in \mathcal{J}}{\text{argmax}} f_{\text{ave}}^\gamma(\tilde{\mathbf{q}}_j), \quad (35a)$$

$$\text{subject to } \mathcal{J} = \left\{ j \mid |p^{\text{min}} - \tilde{p}_j| \leq \varepsilon \right\}, \quad (35b)$$

where $f_{\text{ave}}^\gamma(\mathbf{q})$ is the average RSNR from (23), which is expressed as

$$f_{\text{ave}}^\gamma(\mathbf{q}) = \frac{\gamma_{\text{tx}} N_a^2 (1 - p_{\text{blk}})}{N_t (\kappa + 1) (L - 1)} (\kappa (L - 1) q_1^2 + q_2^2 + \dots + q_L^2). \quad (36)$$

This optimization can also be solved through brute-force search, as in the optimization problem (32) in the previous subsection.

D. Evaluation of Computational Complexity

As described in the previous subsection, the proposed algorithm exhaustively searches all patterns of panel allocation based on the brute-force search. From (31), the order of the panel allocation patterns is $O((N_p + L)!)$. Thus, combinatorial explosion might occur when the number of panels N_p and the number of paths L are large. However, as the parameters N_p and L assume relatively small values, approximately between 1 and 10, in practical mmWave scenarios [18], [43], it is feasible to solve the optimization problem with reasonable complexity even when employing the brute force search.

To evaluate the computational burden of the proposed algorithms, Fig. 6 illustrates the total number of allocation patterns C under various parameter settings for N_p and L , where the number of antenna elements per panel is set to $N_a = 32$ and the total number of antenna elements is $N_t = N_a N_p \in [64, 512]$. As shown in the figure, the number of allocation patterns is at most 10^6 under practical parameter settings. Thus, the optimization problem can be solved with reasonable complexity in the considered mmWave system. Furthermore, the proposed panel allocation algorithms require only long-term statistics, such as the number of paths and the Rician K -factor, without the need for instantaneous CSI. Therefore, it is not required to solve the optimization problem at every channel coherence time, which significantly mitigates the complexity requirements in terms of implementation.

VI. PERFORMANCE ASSESSMENT

This section evaluates the performance of the proposed analog beam designs. The simulation parameters used in this paper are as follows. The carrier frequency f_c is set to 28 GHz,

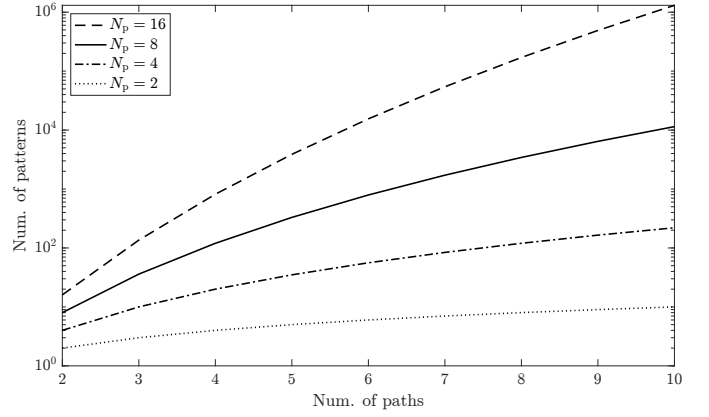


Fig. 6: The total number of allocation patterns C as a function of L . The number of antennas per panel is $N_a = 32$, and the total number of antennas is $N = N_a N_p \in [64, 512]$.

and the system bandwidth W is 400 MHz. The Rician K -factor κ is assumed to be 10 dB [42], and the number of paths L is set to 4. This simulation considers a multi-panel array configuration, where the number of panels N_p is 8, and each panel consists of $N_a = 32$ antenna elements. The hyper parameter of Alg. 2 is set to $\varepsilon = 0.05$. Unless otherwise specified, the transmit SNR is set to $\gamma_{\text{tx}} = 10$ [dB] in the following simulations.

In simulations, the path blockage probability \hat{p} is set to $\hat{p} \sim \mathcal{U}(0.2, 0.6)$ [19], [20] with the average blockage probability $p_{\text{blk}} = 0.4$, and the path blockage parameter ω_l is calculated as

$$\Pr\{\omega_l = 1/\eta\} = \hat{p} \quad (\text{Blocked}), \quad (37a)$$

$$\Pr\{\omega_l = 1\} = 1 - \hat{p} \quad (\text{Otherwise}), \quad (37b)$$

where η denotes the path blockage attenuation and it is defined as $\eta = 9.8 + 180^\circ/A_{\text{BW}}$ with half power beamwidth (HPBW) of analog beamforming A_{BW} [deg] [17].

The system performance is evaluated by CDF of SE, average SE and outage probability of SE. Note that, the SE, outage probability and average SE are defined in (11), (20) and (26), respectively.

To clarify the effectiveness of the proposed beam designs, the following four methods are accessed in the simulation.

- 1) **LoS Concentration** : This method is the commonly used beam design that generate a sharp beam aligns to the LoS path between the BS and UE. This beam design is adopted in current systems, where all panels are coordinated to direct the beam toward a single LoS path [12]–[14].
- 2) **Uniform Path Allocation** : This method allocates panels equally across all paths, not only including LoS path but also NLoS paths. This naive panel allocation is used in the conventional works [27]–[29].
- 3) **OutMin** : This method is the proposed approach presented in Alg. 1, which focuses solely on minimizing the outage probability.
- 4) **OutMin w/ Average SE** : This method is the proposed approach presented in Alg. 2, which considers both the outage probability and the average SE.

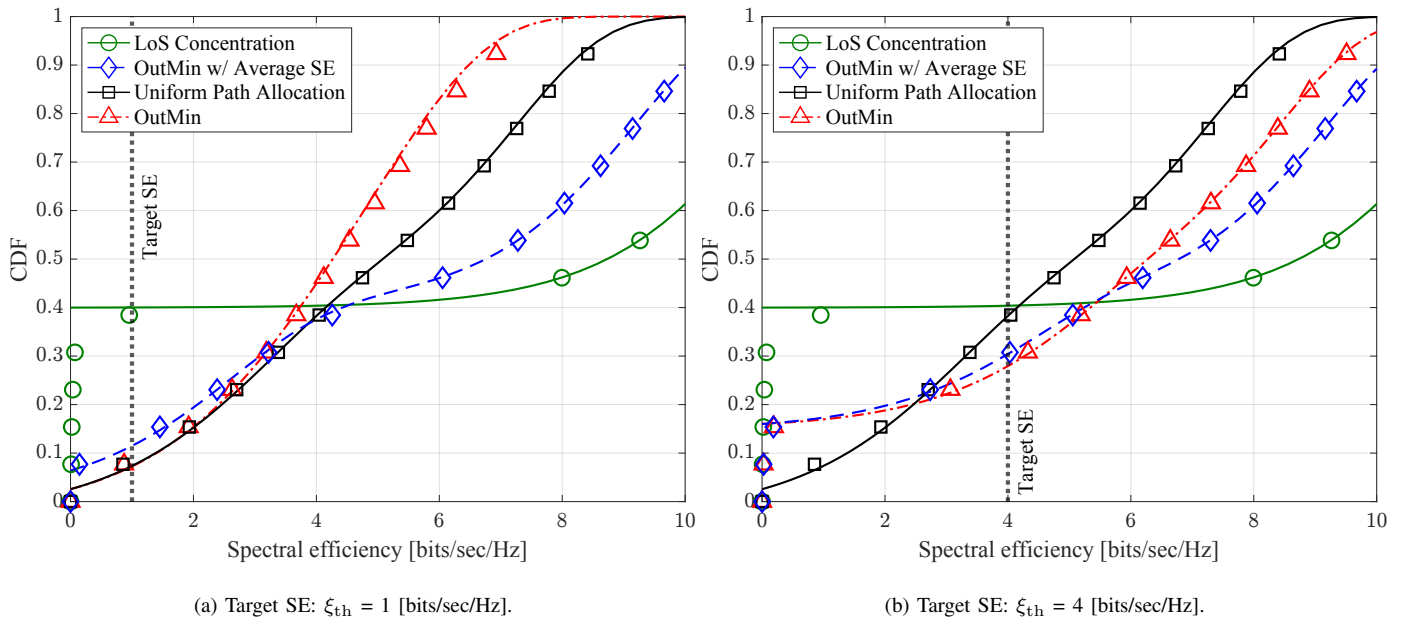


Fig. 7: CDF of the SE for Multiple Target SE. The solid lines represent the analytically calculated CDFs, while the markers indicate the simulated CDFs.

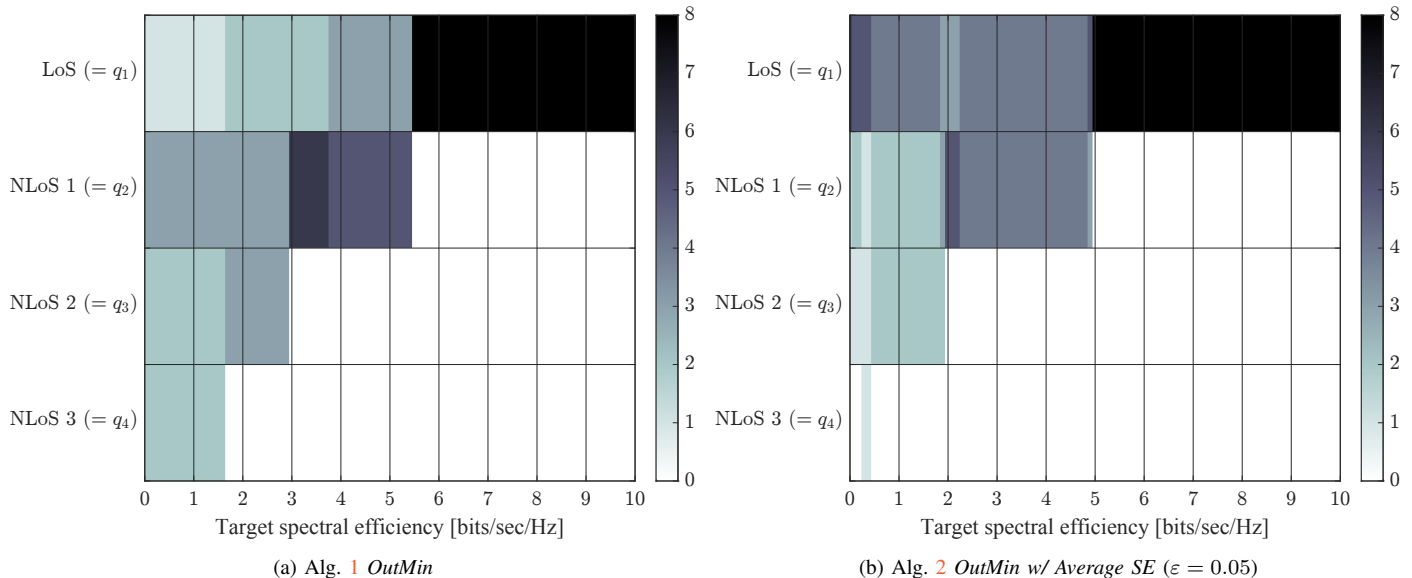
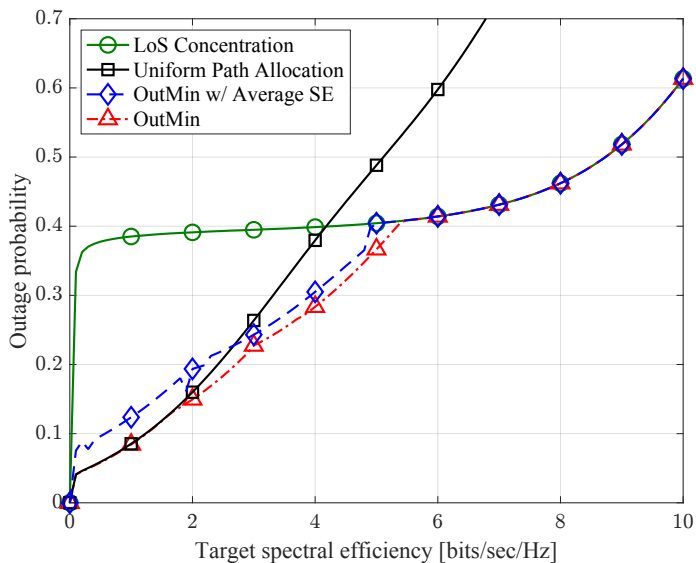


Fig. 8: Panel allocation results in the proposed methods. The vertical axis represents the number of panels aligned to each path, corresponding to each element of \mathbf{q}^{opt} (e.g. $q_1 = 3$ and $q_2 = 1$ indicate that the number of panels aligned to the LoS and NLoS 1 are three and one, respectively)

Hereafter, numerical evaluations are provided based on the aforementioned metrics. First, to validate the theoretical analysis of the SE, the analytically derived CDF of the SE is compared with simulation results in Section VI-A. Subsequently, the outage probability of the SE and the average SE are evaluated as a function of the target SE in Section VI-C. Furthermore the average SE under various SNR conditions is evaluated in Section VI-D. Finally, the results of panel allocation obtained using the two proposed algorithms are presented, and the robustness of the beam design under path blockages is discussed in Section VI-B.

A. Theoretical Analyses for the CDF of the SE

We evaluate the behavior of the CDF of the SE by comparing the analytically calculated CDF with the numerically computed CDF from Monte Carlo simulations with realistic model parameters. The CDFs are shown in Fig. 7a and Fig. 7b, where the target SE values are set to $\xi_{th} = 1$ and 4 [bits/sec/Hz], respectively. The solid lines represent the analytically calculated CDFs, while the markers indicate the numerically computed CDFs. In regions with low SE, there are some discrepancy between the theoretical and simulation results. However, in most other regions, the accuracy of the theoretical analysis is validated, even with utilizing the approximation of the equivalent array response in (14). The discrepancy in the small SE region is attributed to modeling errors in the path blockage.


 Fig. 9: Outage probability as a function of target SE ξ_{th}

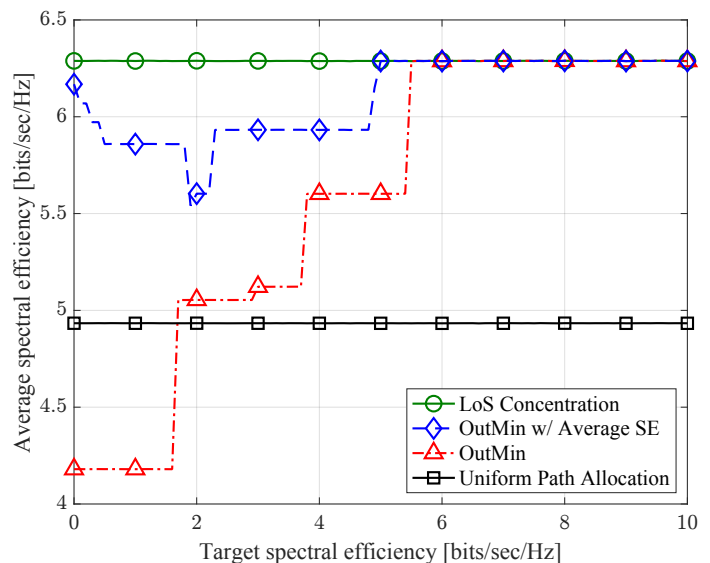
In the theoretical analysis, as indicated in (4), the path gain during blockage is assumed to be zero. However, in practical scenarios, signals can diffract around obstacles when the path is blocked, leading to significant attenuation rather than a complete loss of the path gain. Consequently, the pessimistic assumption of blocked path gain in the theoretical analysis leads to the discrepancy between the theoretical and simulation results.

Compared to the proposed methods, the conventional method, *LoS Concentration*, has a high probability (approximately 0.4) of the SE being 0 [bits/sec/Hz], which is equivalent to the average blockage probability p_{blk} . This result indicates that focusing only on the LoS path results in frequent disconnections whenever the LoS path is blocked, leading to unstable communication. In contrast, the proposed methods and *Uniform Path Allocation*, which utilize multiple paths, can reduce the probability of the SE being 0 [bits/sec/Hz]. Especially in *Uniform Path Allocation*, the probability becomes $p_{blk}^L = 0.0256$ since this method utilizes all L paths. Therefore, unless all the paths are blocked, the communication is not disconnected. This is also verified by the theoretical CDF expressed in (19), where the probability of the SE ξ being zero (i.e., the RSNR γ being zero) is given as p_{blk}^L when $N_b = L$.

Furthermore, the proposed method, *OutMin*, achieve the lowest CDF value at the target SE, demonstrating their flexibility in beam design to handle path blockages. Focusing on Fig. 7a, it is observed that the performance of *OutMin* deteriorates at high SE. This degradation arises because the beams designed by *OutMin* focus solely on minimizing the outage probability without considering the average SE. In comparison, *OutMin w/ Average SE* can suppress the degradation of the average SE by incorporating mechanisms to enhance the average SE as described in Section V-C.

B. Panel Allocation Results

To visualize the optimized panel allocation under various target SE values, we offer, in Fig. 8, the panel allocation


 Fig. 10: Average SE as a function of target SE ξ_{th}

results in the proposed methods, (a) *OutMin* and (b) *OutMin w/ Average SE*. In the figure, the vertical axis represents the number of panels aligned to each path, corresponding to each element of \mathbf{q}^{opt} (e.g. $q_1 = 3$ and $q_2 = 1$ indicate that the number of panels aligned to the LoS and NLoS 1 are three and one, respectively). As shown in the figure, the proposed algorithms generate beams depending on the target SE. In the high target SE region, a single sharp beam focused solely on the LoS path is designed, whereas in the low target SE region, multiple beams aligned with both LoS and NLoS paths are designed. Comparing *OutMin* in Fig. 8a and *OutMin w/ Average SE* in Fig. 8b, both methods utilize multiple paths, however, differences are observed in the number of panels allocated to each path. In *OutMin*, more panels are allocated to NLoS paths than to the LoS path. This is because *OutMin* suppresses the imbalance in the equivalent path gains g_{q_i} for each path in (15) to obtain the higher spatial diversity. In contrast, *OutMin w/ Average SE* allocates more panels to the LoS path than to NLoS paths to improve the average SE by tolerating some degradation in the outage probability. For the same target SE, *OutMin w/ Average SE* tends to reduce the number of beams N_b compared to *OutMin* to obtain high-gain beams for fewer paths rather than to achieve spatial diversity.

C. Outage Probability and Average SE vs. Target SE

To evaluate the outage probability defined in (26), Fig. 9 shows the outage probability as a function of the target SE ξ_{th} . For low target SE values, the conventional method, *LoS Concentration*, experiences outages with a probability equal to the path blockage probability $p_{blk} = 0.4$ due to LoS blockage. In contrast, the proposed methods can suppress the outage probability by exploiting multiple paths. Notably, in the region where the target SE is approximately $\xi_{th} \geq 3$ [bits/sec/Hz], the proposed algorithms in Alg. 1 reduce the outage probability effectively compared to *Uniform Path Allocation* owing to utilizing the LoS path as shown in Fig. 8. The proposed method using Alg. 2 allows an outage probability degradation

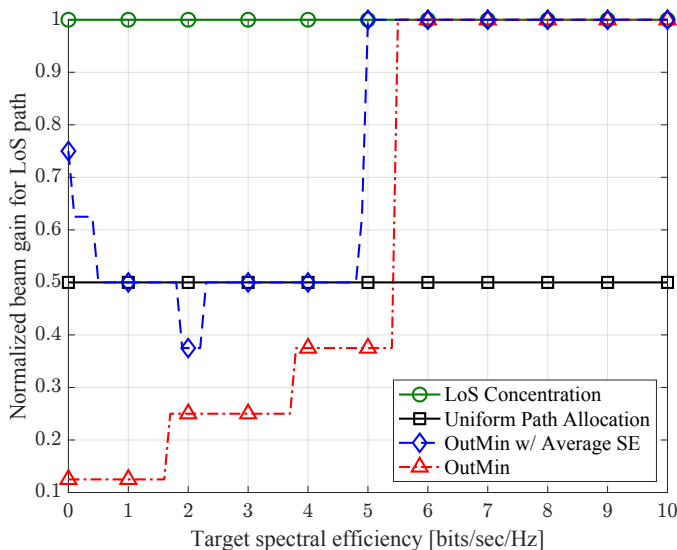


Fig. 11: Normalized beam gain G_{LoS} for LoS path as a function of target SE ξ_{th}

of up to ε to improve the average SE. As a result, the outage probability is degraded by at most ε compared to the result of Alg. 1. To achieve a high target SE, beams must be concentrated on the LoS path. Thus, *LoS Concentration* achieves the lowest outage probability at the high target SE region. The proposed methods achieve spatial diversity in the low target SE region by utilizing multiple beams aligned with multiple paths, and obtain array gain in the high target SE region by focusing beams on the LoS path, thereby suppressing the outage probability for all target SE values.

To evaluate the average SE performance under various the target SE values ξ_{th} , Fig. 10 illustrates the variation of the average SE with respect to the target SE ξ_{th} , where the average SE is evaluated as $\mathbb{E}[\xi] = \mathbb{E}[\log_2(1 + \gamma)]$ defined in (20). As shown in the figure, *LoS Concentration* achieves the highest average SE for any target SE, while *Uniform Path Allocation*, which utilizes multiple paths, fails to achieve improvements in the averaged SE. In contrast, since the proposed methods optimize panel allocation to adapt to the target SE, the average SE varies with the target SE and improves at higher target SE values. Comparing the outage probability in Fig. 9 and the average SE in Fig. 10, it can be seen that there is a trade-off between them in the low target SE region, where the outage probability can be improved at the cost of the average SE by designing multiple beams. On the other hand, in the high target SE region, the average SE improves by concentrating beams only on the LoS path to obtain array gain, resulting in the improvement of the outage probability.

In Fig. 10, *OutMin w/ Average SE* exhibits a non-monotonic variation in the average SE. To clarify the cause of this behavior, we offer Fig. 11, which illustrates the normalized beam gain for the LoS path G_{LoS} as a function of the target SE ξ_{th} . The normalized beam gain for the LoS path G_{LoS} is defined as

$$G_{\text{LoS}} \triangleq \frac{q_1 N_a}{\sum_{i=1}^L q_i N_a} = \frac{q_1}{N_p}, \quad (38)$$

where q_i is the i -th element of the panel allocation vector \mathbf{q} , and q_1 means the number of beams aligned to the LoS path. Since the beam gain for the i -th path is expressed as $N_a q_i$, the normalized beam gain for the LoS path can be expressed as (38). In the region with low target SE ($\xi_{\text{th}} \leq 2$), it is necessary to utilize multiple paths including both LoS and NLoS paths to achieve the target SE. If the target SE is extremely low, this target SE can be achieved with high probability by utilizing multiple paths, even when most of beams are concentrated on the LoS path. However, as the target SE increases, the required beam gain for NLoS paths to achieve the target SE increases. As a result, the normalized beam gain for the LoS path G_{LoS} decreases as the target SE ξ_{th} increases when $\xi_{\text{th}} \leq 2$, as shown in Fig. 11. In contrast, when the target SE becomes sufficiently high, the use of NLoS paths with small path gains are insufficient for achieving the high target SE, resulting in all beams being concentrated primarily on the LoS path. Thus, when $\xi \geq 2$, the normalized beam gain G_{LoS} increases with the target SE, converging to the result of *LoS concentration*.

D. Transmit SNR vs. Average RSNR and SE

To evaluate the average RSNR and the average SE under various transmit SNR γ_{tx} , Fig. 12 and Fig. 13 present the average RSNR and SE as a function of γ_{tx} . From Fig. 12, it is observed that the conventional method, *LoS Concentration*, achieves the highest average RSNR for all SNR values. This is because *LoS Concentration* is the optimal solution of the average RSNR maximization (24) as described in Section V-A. On the other hand, *OutMin* demonstrates the lowest RSNR performance because this method considers only the outage minimization without accounting for the average RSNR. Meanwhile, *OutMin w/ Average SE* can improve the average RSNR close to that of *LoS Concentration*, while significantly reducing the outage probability, as shown in Fig. 9.

When comparing Fig. 12 and Fig. 13, *LoS Concentration* outperforms *OutMin w/ Average SE* in terms of the average RSNR but underperforms in terms of the average SE. As described in Section V-A, *LoS Concentration* is designed to maximize the upper bound of the average SE, derived from Jensen's inequality in (20), which is equivalent to maximizing the average RSNR. Due to the maximization of the upper bound instead of directly maximizing the average SE, *LoS Concentration* is inferior to *OutMin w/ Average SE* in the average SE performance. *OutMin w/ Average SE* can improve the average SE performance, even when the LoS path is blocked, by utilizing multiple paths. Consequently, designing multiple beams across multiple paths enables improving the SE while reducing the outage probability owing to spatial diversity.

From these simulation results and theoretical analysis, the effectiveness of the proposed analog beam designs are validated in terms of achieving spatial diversity and beam gain under various target SE and SNR values.

VII. CONCLUSION

This paper proposed the analog beamforming designs with multi-panel arrays to enable stable mmWave communications

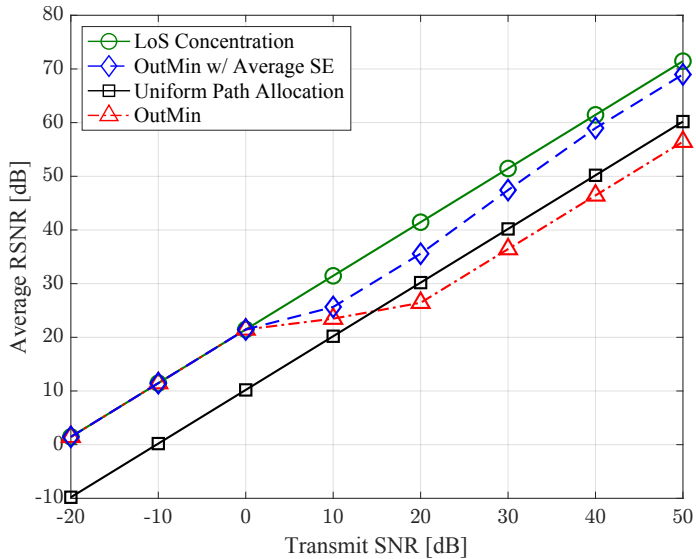


Fig. 12: Average RSNR $\mathbb{E}[\gamma]$ as a function of transmit SNR γ_{tx} : Target SE $\xi_{th} = 4$ [bits/sec/Hz]

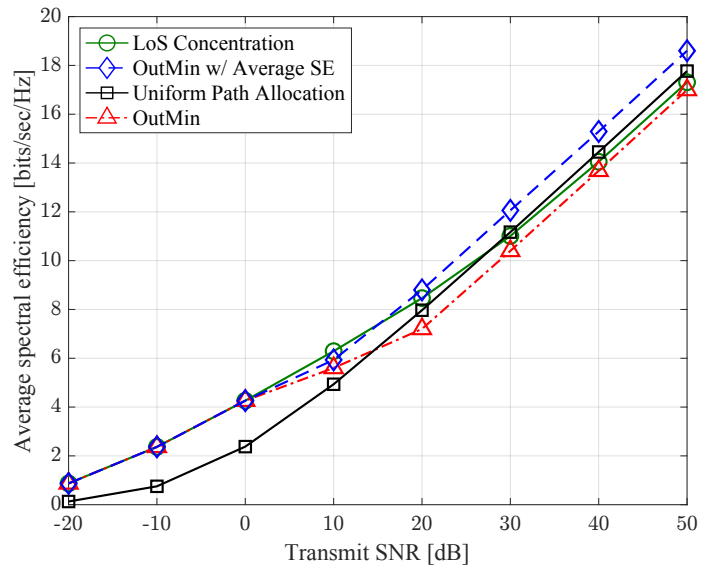


Fig. 13: Average SE $\mathbb{E}[\xi]$ as a function of transmit SNR γ_{tx} : Target SE $\xi_{th} = 4$ [bits/sec/Hz]

under stochastic blockages. We provided the theoretical analysis of SE and formulated the outage probability minimization problem for panel allocation.

The theoretical analysis derived the closed-form expressions for the CDF and outage probability of SE in multi-beam design employing multi-panel arrays. By approximating the array response, the outage probability of SE and the RSNR were derived in closed form. To optimize panel allocation, two analog beamforming algorithms were proposed: one focused on minimizing outage probability and the other jointly optimizing outage probability and average SE. The panel allocation problem was formulated as a combinatorial optimization problem that determines the assignment of panels to both LoS and NLoS paths. The proposed algorithm requires only long-term statistical information, such as the number of paths and the Rician K -factor, eliminating the need for instantaneous CSI. Thus, the optimization does not need to be solved at every channel coherence time, simplifying implementation.

The effectiveness of the theoretical analysis and the proposed beamforming designs was validated through computational simulations using realistic mmWave parameters. The results demonstrated that conventional LoS-concentrated beamforming, while optimal for maximizing average RSNR, frequently degrades communication quality. In contrast, the proposed multi-beam approach, which utilizes both LoS and NLoS paths, effectively suppresses outage probability and ensures more stable communication compared to conventional methods. From these results, proposed multiple wide beam design achieves stable communication over stochastic blockages, outperforming the conventional single sharp-beam design.

APPENDIX A

DERIVATION OF THE EQUIVALENT CHANNEL RESPONSE

We derive the PDF of the equivalent channel response h_{eq} in (16). According to the approximation in (15), the equivalent

channel response is represented as sum of $g_{q_l}\omega_l$ where, g_{q_l} and ω_l denote the circular symmetric complex Gaussian and Bernoulli random variable. Since $g_{q_l}\omega_l$ is also expressed as a Bernoulli-Gaussian random variable, h_{eq} can be represented as a Bernoulli-Gaussian mixture random variable. The equivalent channel response h_{eq} in (15) can be reformulated as

$$h_{eq} = \frac{N_a}{\sqrt{N_t}} \sum_{l \in \mathcal{L}} g_{q_l} \omega_l = \frac{N_a}{\sqrt{N_t}} \sum_{l \in \mathcal{L}} e_l, \quad (39)$$

where e_l is a dominant component of the equivalent channel response at the l -th path and it follows the Bernoulli-Gaussian distribution. Here, the PDFs of g_{q_l} , ω_l and e_l are defined as

$$f_{G_{q_l}}(g_{q_l}) = \mathcal{CN}(g_{q_l}; 0, \rho_l^2) = \frac{1}{\pi \rho_l^2} \exp\left(-\frac{|g_{q_l}|^2}{\rho_l^2}\right), \quad (40)$$

$$f_{\Omega_l}(\omega_l) = \mathcal{B}(\omega_l; p_{blk}) = p_{blk}^{1-\omega_l} (1-p_{blk})^{\omega_l}, \quad (41)$$

$$f_{E_l}(e_l) = p_{blk} \delta(e_l) + (1-p_{blk}) f_{G_{q_l}}(e_l). \quad (42)$$

According to the equation (39) h_{eq} is represented as the sum of Bernoulli-Gaussian random variables e_l , h_{eq} follows the Bernoulli-Gaussian mixture distribution. Since e_l is independent for each l , the PDF of h_{eq} can be calculated as the convolution product of the PDFs of each equivalent response e_l . Thus, the PDF of the h_{eq} can be written as

$$f_{H_{eq}}(h_{eq}) = f_{E_1}(e_1) \otimes f_{E_2}(e_2) \otimes \cdots \otimes f_{E_L}(e_L). \quad (43)$$

Furthermore, by simplifying the equation (43), we obtain the PDF of the equivalent channel response as in (16).

APPENDIX B

DERIVATION OF THE RSNR DISTRIBUTION

We derive the PDF and CDF of the RSNR written in (18), (19). As shown in (17), the RSNR γ is expressed as the square of the equivalent channel response $|h_{eq}|^2$, which corresponds to the square of a Bernoulli-Gaussian mixture

random variable. In the following, the objective is to derive the PDF of the RSNR, *i.e.*, the distribution of the square of a Bernoulli-Gaussian mixture random variable.

The mixture distribution shown in (16) is expressed as the sum of a δ -function term derived from the Bernoulli distribution and multiple complex Gaussian distributions, represented as a weighted sum with respect to the power of p_{blk} . As each distribution does not have cross terms, the squared distribution can be calculated separately for each distribution. First, the squared distribution of the complex Gaussian distribution is calculated. Let $x \sim \mathcal{CN}(0, \rho^2)$ be a Gaussian random variable, and its PDF is expressed as

$$f_X(x) = \mathcal{CN}(x; 0, \rho^2) = \frac{1}{\pi\rho^2} \exp\left(-\frac{|x|^2}{\rho^2}\right). \quad (44)$$

Let x be defined as $x = x_r + jx_i$, where $x_r = r \cos \theta$ and $x_i = r \sin \theta$. Using this variable transformation, the PDF of the random variable $y = |x|^2 \geq 0$ is expressed as

$$\begin{aligned} f_Y(y) &= \int_0^{2\pi} \int_0^\infty f_X(r, \theta) \delta(y - r^2) r dr d\theta, \\ &= \int_0^{2\pi} \int_0^\infty \frac{1}{\pi\rho^2} \exp\left(-\frac{r^2}{\rho^2}\right) \delta(y - r^2) r dr d\theta, \\ &= \int_0^{2\pi} \int_0^\infty \frac{1}{\pi\rho^2} \exp\left(-\frac{r^2}{\rho^2}\right) \frac{1}{2\sqrt{y}} \delta(r - \sqrt{y}) r dr d\theta, \\ &= \int_0^{2\pi} \frac{1}{\pi\rho^2} \exp\left(-\frac{y}{\rho^2}\right) \frac{1}{2\sqrt{y}} \sqrt{y} d\theta, \\ &= \frac{1}{\pi\rho^2} \exp\left(-\frac{y}{\rho^2}\right) \frac{\sqrt{y}}{2\sqrt{y}} \cdot 2\pi, \\ &= \frac{1}{\rho^2} \exp\left(-\frac{y}{\rho^2}\right), \end{aligned} \quad (45)$$

where the property of the δ -function is utilized, and the transformation $\delta(y - r^2) = \frac{1}{2\sqrt{y}} \delta(r - \sqrt{y})$ is applied. Therefore, the Gaussian distribution component can be expressed as a weighted sum of exponential distributions. Additionally, for the δ -function component in (16), squaring it still results in a δ -function. Consequently, the PDF of the RSNR γ , which follows the squared Bernoulli-Gaussian mixture distribution, can be expressed as shown in (18).

Subsequently, we rewrite the PDF shown in (18) as a CDF. This can also be determined by independently calculating the CDF for each distribution and then computing their weighted sum, which can be expressed as (19).

REFERENCES

[1] Y. Heng, J. G. Andrews, J. Mo, V. Va, A. Ali, B. L. Ng, and J. C. Zhang, "Six key challenges for beam management in 5.5G and 6G systems," *IEEE Commun. Mag.*, vol. 59, no. 7, pp. 74–79, Jul. 2021.

[2] F. Tang, X. Chen, M. Zhao, and N. Kato, "The roadmap of communication and networking in 6G for the metaverse," *IEEE Wireless Commun.*, vol. 30, no. 4, pp. 72–81, Jun. 2022.

[3] M. Maier, "6G as if People Mattered: From Industry 4.0 toward Society 5.0 : (Invited Paper)," in *Proc. Int. Conf. Comput. Commun. Netw. (ICCCN)*, Jul. 2021, pp. 1–10.

[4] M. Z. Chowdhury, M. Shahjalal, S. Ahmed, and Y. M. Jang, "6G wireless communication systems: Applications, requirements, technologies, challenges, and research directions," *IEEE Open J. Commun. Soc.*, vol. 1, pp. 957–975, Jul. 2020.

[5] T. S. Rappaport, G. R. MacCartney, M. K. Samimi, and S. Sun, "Wide-band millimeter-wave propagation measurements and channel models for future wireless communication system design," *IEEE Trans. Commun.*, vol. 63, no. 9, pp. 3029–3056, May 2015.

[6] R. W. Heath, N. Gonzalez-Prelcic, S. Rangan, W. Roh, and A. M. Sayeed, "An overview of signal processing techniques for millimeter wave MIMO systems," *IEEE J. Sel. Topics Signal Process.*, vol. 10, no. 3, pp. 436–453, Feb. 2016.

[7] E. G. Larsson, O. Edfors, F. Tufvesson, and T. L. Marzetta, "Massive MIMO for next generation wireless systems," *IEEE Commun. Mag.*, vol. 52, no. 2, pp. 186–195, Feb. 2014.

[8] R1-1611666, "Codebook design for multi-panel structured MIMO in NR," *GPP TSG RAN WG1-86, Reno, US*, 2016.

[9] Y. Huang, Y. Li, H. Ren, J. Lu, and W. Zhang, "Multi-panel MIMO in 5G," *IEEE Commun. Mag.*, vol. 56, no. 3, pp. 56–61, Mar. 2018.

[10] N. Song, P. Wen, H. Sun, and T. Yang, "Multi-panel based hybrid beamforming for multi-user massive mimo," in *Proc. IEEE Global Commun. Conf. (GLOBECOM)*, IEEE, 2017, pp. 1–6.

[11] W. Wang and W. Zhang, "Truncated tree based hybrid beamforming for multi-panel MIMO," *IEEE Trans. Veh. Technol.*, vol. 69, no. 11, pp. 13 974–13 978, Nov. 2020.

[12] 3rd Generation Partnership Project (3GPP), "Study on new radio (NR) access technology," 3GPP, Tech. Rep. 38.912, 2018.

[13] —, "Summary of CSI enhancements for MTRP and FDD," 3GPP, Tech. Rep. R1-210abcd, 2020.

[14] —, "NR; Physical layer procedures for data," 3GPP, Tech. Rep. 38.214, 2019.

[15] S. Mukherjee, G. Skidmore, T. Chawla, A. Bhardwaj, C. Gentile, and J. Senic, "Scalable modeling of human blockage at millimeter-wave: A comparative analysis of knife-edge diffraction, the uniform theory of diffraction, and physical optics against 60 GHz channel measurements," *IEEE Access*, vol. 10, pp. 133 643–133 654, Dec. 2022.

[16] C. Slezak, V. Semkin, S. Andreev, Y. Koucheryavy, and S. Rangan, "Empirical effects of dynamic human-body blockage in 60 GHz communications," *IEEE Commun. Mag.*, vol. 56, no. 12, pp. 60–66, Dec. 2018.

[17] G. R. MacCartney, T. S. Rappaport, and S. Rangan, "Rapid fading due to human blockage in pedestrian crowds at 5G millimeter-wave frequencies," in *Proc. IEEE Global Commun. Conf. (GLOBECOM)*, IEEE, Dec 2017, pp. 1–7.

[18] M. R. Akdeniz, Y. Liu, M. K. Samimi, S. Sun, S. Rangan, T. S. Rappaport, and E. Erkip, "Millimeter wave channel modeling and cellular capacity evaluation," *IEEE J. Sel. Areas Commun.*, vol. 32, no. 6, pp. 1164–1179, Jun. 2014.

[19] T. S. Rappaport, G. R. MacCartney, M. K. Samimi, and S. Sun, "Wide-band millimeter-wave propagation measurements and channel models for future wireless communication system design," *IEEE Trans. Commun.*, vol. 63, no. 9, pp. 3029–3056, Sep. 2015.

[20] V. Raghavan *et al.*, "Statistical blockage modeling and robustness of beamforming in millimeter-wave systems," *IEEE Trans. Microw. Theory Techn.*, vol. 67, no. 7, pp. 3010–3024, Jul. 2019.

[21] K. Li, H. Xu, X. Wang, and K. Ishibashi, "Human blockage analysis at 5G millimeter wave frequencies using a high-resolution voxel model," in *Proc. IEEE VTS Asia Pacific Wireless Commun. Symp. (APWCS)*, IEEE, Aug. 2024, pp. 1–5.

[22] H. Iimori, G. T. F. de Abreu, O. Taghizadeh, R.-A. Stoica, T. Hara, and K. Ishibashi, "Stochastic learning robust beamforming for millimeter-wave systems with path blockage," *IEEE Wireless Commun. Lett.*, vol. 9, no. 9, pp. 1557–1561, May 2020.

[23] S. Uchimura, H. Iimori, G. T. F. de Abreu, and K. Ishibashi, "Outage-minimization coordinated multi-point for millimeter-wave OFDM with random blockages," *IEEE Trans. Veh. Technol.*, 2023.

[24] S. Uchimura, G. T. F. De Abreu, and K. Ishibashi, "Blockage-robust hybrid beamforming enabling high sum rate for millimeter-wave OFDM systems," *IEEE Trans. Wireless Commun.*, pp. 1–1, Dec. 2023.

[25] S. Uchimura, G. T. F. de Abreu, and K. Ishibashi, "Hybrid beamforming for outage-minimization in frequency selective millimeter-wave channels," in *Proc. IEEE Wireless Commun. Netw. Conf. (WCNC)*, IEEE, Mar. 2023, pp. 1–6.

[26] S. Doğan, M. Karabacak, and H. Arslan, "Optimization of antenna beamwidth under blockage impact in millimeter-wave bands," in *Proc. IEEE 29th Annu. Int. Symp. Pers., Indoor Mobile Radio Commun. (PIMRC)*, Sep. 2018, pp. 1–5.

[27] I. K. Jain, R. Subbaraman, and D. Bharadia, "Two beams are better than one: Towards reliable and high throughput mmwave links," in *Proc. ACM SIGCOMM 2021 Conf.*, 2021, pp. 488–502.

- [28] S. K. Wilson, M. Stojanovic, M. Médard, and K. Schab, "Random guessing for beam alignment: A low complexity strategy for reducing blockage in mmwave communications," *IEEE Access*, vol. 10, pp. 80 989–80 998, 2022.
- [29] K. Terui, K. Arai, and K. Ishibashi, "Robust beamforming with multi-panel array for mmWave channels over mobility and blockage," in *Proc. IEEE 100th Veh. Technol. Conf. (VTC2024-Fall)*. IEEE, Oct 2024, pp. 1–5.
- [30] D. Kumar, S. K. Joshi, and A. Tölli, "Latency-aware highly-reliable mmwave systems via multi-point connectivity," *IEEE Access*, vol. 10, pp. 32 822–32 835, Mar. 2022.
- [31] D. Kumar, J. Kaleva, and A. Tölli, "Blockage-aware reliable mmWave access via coordinated multi-point connectivity," *IEEE Trans. Wireless Commun.*, vol. 20, no. 7, pp. 4238–4252, Jul. 2021.
- [32] T. Nishio, H. Okamoto, K. Nakashima, Y. Koda, K. Yamamoto, M. Morikura, Y. Asai, and R. Miyatake, "Proactive received power prediction using machine learning and depth images for mmWave networks," *IEEE J. Sel. Areas Commun.*, vol. 37, no. 11, pp. 2413–2427, Nov. 2019.
- [33] W. Wang, W. Zhang, and J. Wu, "Optimal beam pattern design for hybrid beamforming in millimeter wave communications," *IEEE Trans. Veh. Technol.*, vol. 69, no. 7, pp. 7987–7991, May 2020.
- [34] K. Arai and K. Ishibashi, "Self-calibration for channel estimation in hybrid millimeter-wave MIMO systems," in *Proc. IEEE 98th Veh. Technol. Conf. (VTC2023-Fall)*, Oct. 2023, pp. 1–5.
- [35] M. Eberhardt, P. Eschlwech, and E. Biebl, "Investigations on antenna array calibration algorithms for direction-of-arrival estimation," *Advances in Radio Science*, vol. 14, pp. 181–190, Sep. 2016.
- [36] H. Chen, M. F. Keskin, S. R. Aghdam, H. Kim, S. Lindberg, A. Wolfgang, T. E. Abrudan, T. Eriksson, and H. Wymeersch, "Modeling and analysis of OFDM-based 5G/6G localization under hardware impairments," *IEEE Trans. Wireless Commun.*, vol. 23, no. 7, pp. 7319–7333, Dec. 2024.
- [37] W. Wang and W. Zhang, "Orthogonal projection-based channel estimation for multi-panel millimeter wave MIMO," *IEEE Trans. Commun.*, vol. 68, no. 4, pp. 2173–2187, Apr. 2020.
- [38] S. Kamiwatari, I. Kanno, T. Ohseki, K. Yamazaki, and Y. Kishi, "RF chain-wise clustering for centralized mm-wave cell-free massive MIMO with hybrid beamforming," in *Proc. IEEE Global Commun. Conf. (GLOBECOM)*. IEEE, Dec. 2022, pp. 764–769.
- [39] J. Rodríguez-Fernández, N. González-Prelcic, K. Venugopal, and R. W. Heath, "Frequency-domain compressive channel estimation for frequency-selective hybrid millimeter wave MIMO systems," *IEEE Trans. Wireless Commun.*, vol. 17, no. 5, pp. 2946–2960, Mar. 2018.
- [40] R.-A. Stoica, H. Iimori, G. T. Freitas de Abreu, and K. Ishibashi, "Frame theory and fractional programming for sparse recovery-based mmWave channel estimation," *IEEE Access*, vol. 7, pp. 150 757–150 774, Oct. 2019.
- [41] J. L. W. V. Jensen, "Sur les fonctions convexes et les inégalités entre les valeurs moyennes," *Acta mathematica*, vol. 30, no. 1, pp. 175–193, Dec. 1906.
- [42] M. K. Samimi, G. R. MacCartney, S. Sun, and T. S. Rappaport, "28 GHz millimeter-wave ultrawideband small-scale fading models in wireless channels," in *Proc. IEEE 83rd Veh. Technol. Conf. (VTC2016-Spring)*, May 2016.
- [43] I. A. Hemadeh, K. Satyanarayana, M. El-Hajjar, and L. Hanzo, "Millimeter-wave communications: Physical channel models, design considerations, antenna constructions, and link-budget," *IEEE Commun. Surv. Tut.*, vol. 20, no. 2, pp. 870–913, Dec. 2018.